Available online at www.sciencedirect.com
SCIENCE DIRECT®

Journal of the European Ceramic Society 23 (2003) 2671–2675

www.elsevier.com/locate/jeurceramsoc

Microwave dielectric imaging of $Ba_2Ti_9O_{20}$ materials with a scanning-tip microwave near-field microscope

Yi-Chun Chen[a,*], Hsiu-Fung Cheng[a], Gang Wang[b], Xiao-Dong Xiang[b], Yi-Chen Chiang[c], Kuo Shung Liu[c], I-Nan Lin[c]

[a]*Department of Physics, National Taiwan Normal University, Taipei 116, Taiwan, ROC*
[b]*Intematix, Moraga, CA 94556, USA*
[c]*Department of Materials Science & Engineering, Materials Science Center, National Tsing-Hua University, Hsinchu 300, Taiwan, ROC*

Abstract

The dielectric image of $Ba_2Ti_9O_{20}$, B_2T_9, materials at microwave frequencies was measured using a scanning evanescent microwave probe (EMP) technique. The average dielectric constant evaluated from the dielectric image ($\varepsilon_r = 26$–43) was consistent with the measurements made using a conventional cavity method, which are in the range $\varepsilon_r = 32$–38. The dielectric image consists of aggregates of clusters about tens of micron in size, and is totally different from the conventional granular structure for the materials, which contains submicron sized grains. The calcination conditions were observed to impose marked influence on the phase purity and hence the microwave dielectric properties of the sintered materials. EMP-derived dielectric images reveal that the materials containing secondary phases and exhibiting low Q-factor consist of aggregates of clusters with pronounced fluctuated distribution of dielectric constant, whereas the materials of high phase purity and high Q-factor show very mild fluctuation in dielectric constant over the samples.
© 2003 Elsevier Ltd. All rights reserved.

Keywords: $Ba_2Ti_9O_{20}$; Co-precipitation; Dielectric properties; Microwave ceramics; Resonators; Near field spectroscopy

1. Introduction

Among the compounds in the BaO–TiO_2 system, $Ba_2Ti_9O_{20}$ possesses an excellent combination of high quality factor (Q), moderate dielectric constant (ε_r), and most of all, low temperature coefficient of resonant frequency (τ_f) in the microwave frequency region.[1–3] It is therefore a useful material for microwave resonators and has been intensely investigated. However, with a low nucleation rate,[4] $Ba_2Ti_9O_{20}$ does not form as readily as some other BaO–TiO_2 compounds, such as $BaTi_5O_{11}$ and $BaTi_4O_9$. Pure $Ba_2Ti_9O_{20}$ is difficult to be obtained synthetically. In this study, a co-precipitation process is adopted to enhance the formation of the $Ba_2Ti_9O_{20}$ hollandite phase, for the purpose of studying the effect of second phase on the dielectric properties of the materials.

Due to the long wavelength associated with the microwave frequency region, there has not been a sensitive detection system for the dielectric measurement of microstructure at microwave frequencies. Over the years, a variety of near-field scanning microscopes have been developed to probe local variations of properties and the structures of materials, attaining to spatial resolutions of $\lambda/20$–$\lambda/600$.[5] An evanescent microwave probe (EMP) based on a microwave resonator[6–8] has been developed to image surface impedance profiles in microwave frequency region, and spatial resolution is further improved to $\sim$50 nm by using a tip-probe and an efficient shielding structure. To illustrate the connection between the microstructure and the dielectric properties of $Ba_2Ti_9O_{20}$ ceramics, we use EMP to derive the distribution of dielectric constant, i.e. the dielectric image, of the samples directly. The results were also compared with the conventional cavity measurements.

2. Experimental methods

The $Ba_2Ti_9O_{20}$ materials were prepared by the co-precipitation method. The $Ba(OH_2)2H_2O$ and $TiCl_4$ is appropriate ratio (Ba:Ti = 2:9) were dissolved in H_2O, which were then spared into coprecipitants consisting of $NH_4(OH)$ and $(NH_4)_2CO_3$ mixture. The coprecipitates

* Corresponding author.
E-mail address: s41409@cc.ntnu.edu.tw (Y.-C. Chen).

0955-2219/03/$ - see front matter © 2003 Elsevier Ltd. All rights reserved.
doi:10.1016/S0955-2219(03)00181-X

thus obtained were then filtered and washed for several times to get rid of residual NH_4Cl. The coprecipitates were then calcined at 800–1100 °C for 4 h, followed by pulverization, pressing and then sintered at 1300 °C for 4 h (in air).

The crystal structure and microstructure of the sintered samples were examined using X-ray diffraction and scanning electron microscopy. The average microwave dielectric properties of the materials were measured using the conventional cavity method. To investigate the local variation of dielectric properties of the materials, an EMP was used to make nondestructive measurements of the dielectric properties of the samples. The system design consists of a sharpened metal tip, mounted on the centre conductor of a high-Q (quality factor) $\lambda/4$ coaxial resonator, protruding beyond an aperture formed on the end wall of the resonator. The resonator acts as both an evanescent field emitter and a detector. A change in the local environment of the probe leads to a change in the resonant frequency f_0 of the resonator, and the signal is detected by measuring the power response near the resonant frequency. To perform quantitative measurements, perturbation theory was used to analyze the resonant system. From the shift of resonant frequencies (Δf) and the change in resonator's Q-value ($\Delta\frac{1}{Q}$), the dielectric properties of the bulk sample can be analyzed by the following equations:[9]

$$\frac{\Delta f}{f_0} = -\frac{\int_v(\Delta\varepsilon E_1\cdot E_0 + \Delta\mu H_1\cdot H_0)dv}{\int_v(\varepsilon_0 E_0^2 + \mu_0 H_0^2)dv}$$

$$= A\left[\frac{\ln(1-b)}{b} + 1\right] \quad (1)$$

$$\Delta\left(\frac{1}{Q}\right) = -\frac{\int_v(\Delta\varepsilon'' E_1\cdot E_0 + \Delta\mu'' H_1\cdot H_0)dv}{\int_v(\varepsilon_0 E_0^2 + \mu_0 H_0^2)dv}$$

$$= -\left(\frac{1}{Q_0} + 2\tan\delta\right)\frac{\Delta f}{f_0} \quad (2)$$

where $\Delta f = f_r - f_0$, $\Delta\left(\frac{1}{Q}\right) = \frac{1}{Q} - \frac{1}{Q_0}$, f_0 and Q_0 are, respectively, the resonant frequency and quality factor of the resonator without the samples, f_r and Q_r are the measured resonant frequency and quality factor of the resonator with a sample placed in adjacent to the EMP probe. $b = \frac{\varepsilon-\varepsilon_0}{\varepsilon+\varepsilon_0}$, ε is the dielectric constant of the sample, ε_0 is the permittivity of free space, and A is a constant determined by the geometry of the tip-cavity assembly which should be calibrated using standard samples. Due to the favourable field distribution caused by tip-probe ($R_0 \sim 10$ to 100 μm), a small change in field distribution near the tip induces a large change in f_0, and high spatial resolution and high sensitivity are obtained.

3. Results and discussion

The phase purity for the sintered $Ba_2Ti_9O_{20}$ materials is closely related to phase constituent in the as-calcined powders. The $BaTi_5O_{11}$ phase was preferentially formed when the $BaCO_3$–TiO_2 mixture was calcined at 800 or 1000 °C and at calcination temperature of 1100 °C or above the $Ba_2Ti_9O_{20}$ hollandite phase is also formed (Fig. 1a). However, at these temperatures there is still residual $BaTi_5O_{11}$ phase. Most of the intermediate phase can be converted into the hollandite structure by sintering at 1300 °C for 4 h. Fig. 1b shows that the

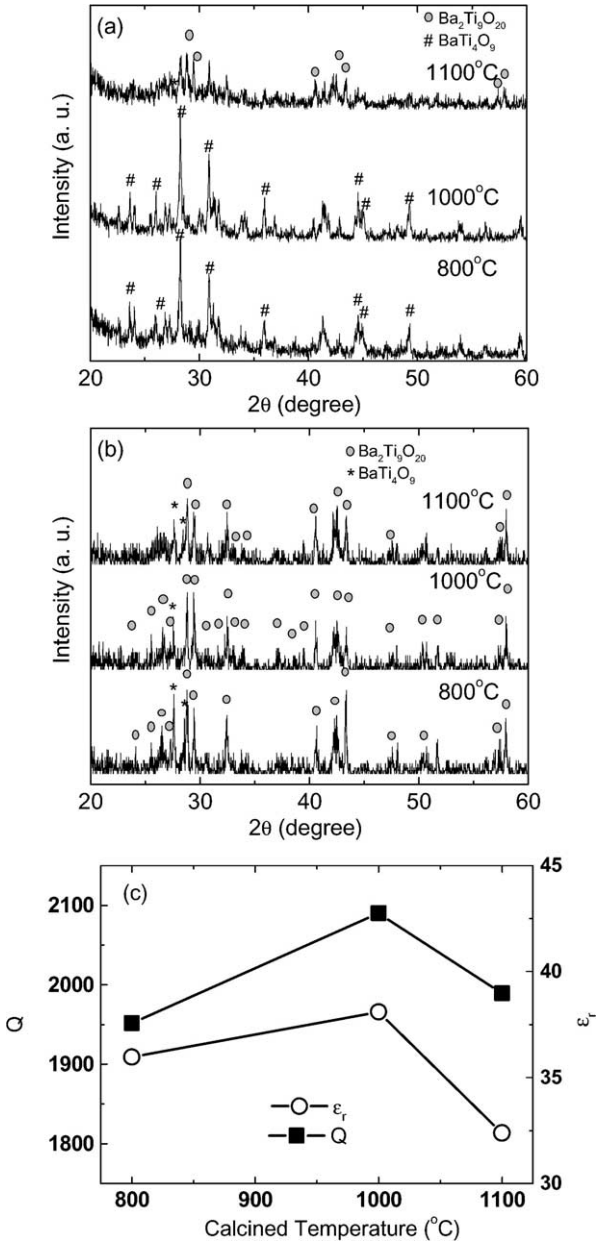

Fig. 1. (a) X-ray diffraction patterns for the as-calcined $Ba_2Ti_9O_{20}$ powders and (b) those for the 1300 °C (4 h) sintered pellets, and (c) microwave dielectric properties (ε_r and Q) measured at 6 GHz of thus obtained $Ba_2Ti_9O_{20}$ materials.

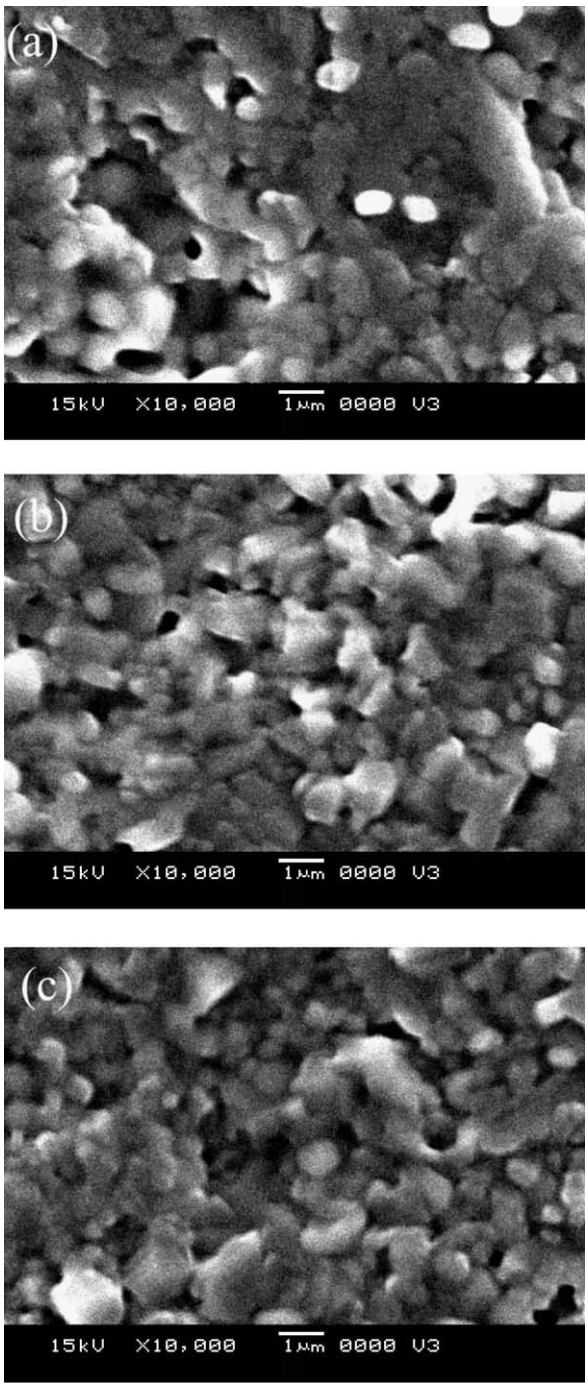

Fig. 2. SEM micrographs for $Ba_2Ti_9O_{20}$ materials prepared from (a) 800 °C, (b) 1000 °C, (c) 1100 °C calcined powders and sintered at 1300 °C (4 h).

ceramics prepared from 1000 °C-calcined powders contain the least amount of secondary phase, whereas those prepared from 800 or 1100 °C-calcined powders contain a large proportion of second phases; mainly the $BaTi_4O_9$ intermediate phase. The diffuse X-ray diffraction peak in the $2\theta = 25$–$30°$ region implies the existence of a complicated second phase for the samples prepared from 1100 °C-calcined powders.

Fig. 1c shows the microwave properties, dielectric constant (ε_r) and quality factor (Q), for the sintered $Ba_2Ti_9O_{20}$ materials, measured by conventional cavity resonator method at 6 GHz. The dielectric properties of the samples are intimately correlated with their phase purity. The 1000 °C-derived $Ba_2Ti_9O_{20}$ samples, which contain highest phase purity, possess largest dielectric constant and highest quality factor ($\varepsilon_r = 38$, $Q = 2090$ at 6 GHz). The microwave properties were markedly degraded for 800 and 1100 °C-derived $Ba_2Ti_9O_{20}$ samples due to the presence of secondary phases.

The SEM micrographs of the sintered materials, shown in Fig. 2a–c, indicate that the microstructures of the three categories of $Ba_2Ti_9O_{20}$ materials are not very much different from one another. All the samples contain uniformly distributed grains of submicron size. The grains in the 800 °C-derived samples are mostly of equiaxed geometry, whereas the 1000 and 1100 °C-derived ones contain some elongated grains. There appear some abnormally larger grains in the 1100 °C-derived samples. The presence of the grains of different shape shown in SEM micrographs and the existence of secondary phases shown in XRD patterns indicate clearly that the undesired phase is of different geometry and is the cause of degradation on the microwave properties. However there are still no measurements that can directly confirm the correlation between the microwave dielectric properties and the microstructure.

To correlate directly the dielectric properties and microstructure in microwave regime, an EMP was used to image the distribution of dielectric properties in the ceramics. The measurement is based on the principle that as the tip approaches the sample surface, the evanescent wave from the tip of a resonator will interact with the sample, inducing the field redistribution. This effect can be modelled by adding an additional capacitive impedance to the resonator, which causes the change in resonator characteristics.

Fig. 3 shows the frequency image (I) measured by EMP and the dielectric image (II) derived using Eqs. (1) and (2) for the samples, which were prepared from the 800 to 1100 °C calcined powders, sintered at 1300 °C for 4 h. The average dielectric constant, about 26–43, is consistent with that measured by the conventional cavity resonator method. For the 1000 °C-calcined $Ba_2Ti_9O_{20}$ samples (Fig. 3b), most of the region examined possesses high dielectric constant ($\varepsilon_r \cong 40$). The variation of dielectric constant over the samples is very limited. Only a few areas show either larger or smaller dielectric constant. In contrast, for 800 °C-derived $Ba_2Ti_9O_{20}$ samples, the dielectric constant varies pronouncedly over the samples, shown as dielectric image in Fig. 3a. Regions of high dielectric (or low dielectric constant) aggregate, forming clusters typically tens of microns in size. Most of the region possesses a dielectric constant of about $\varepsilon_r \cong 32$, which is markedly lower than

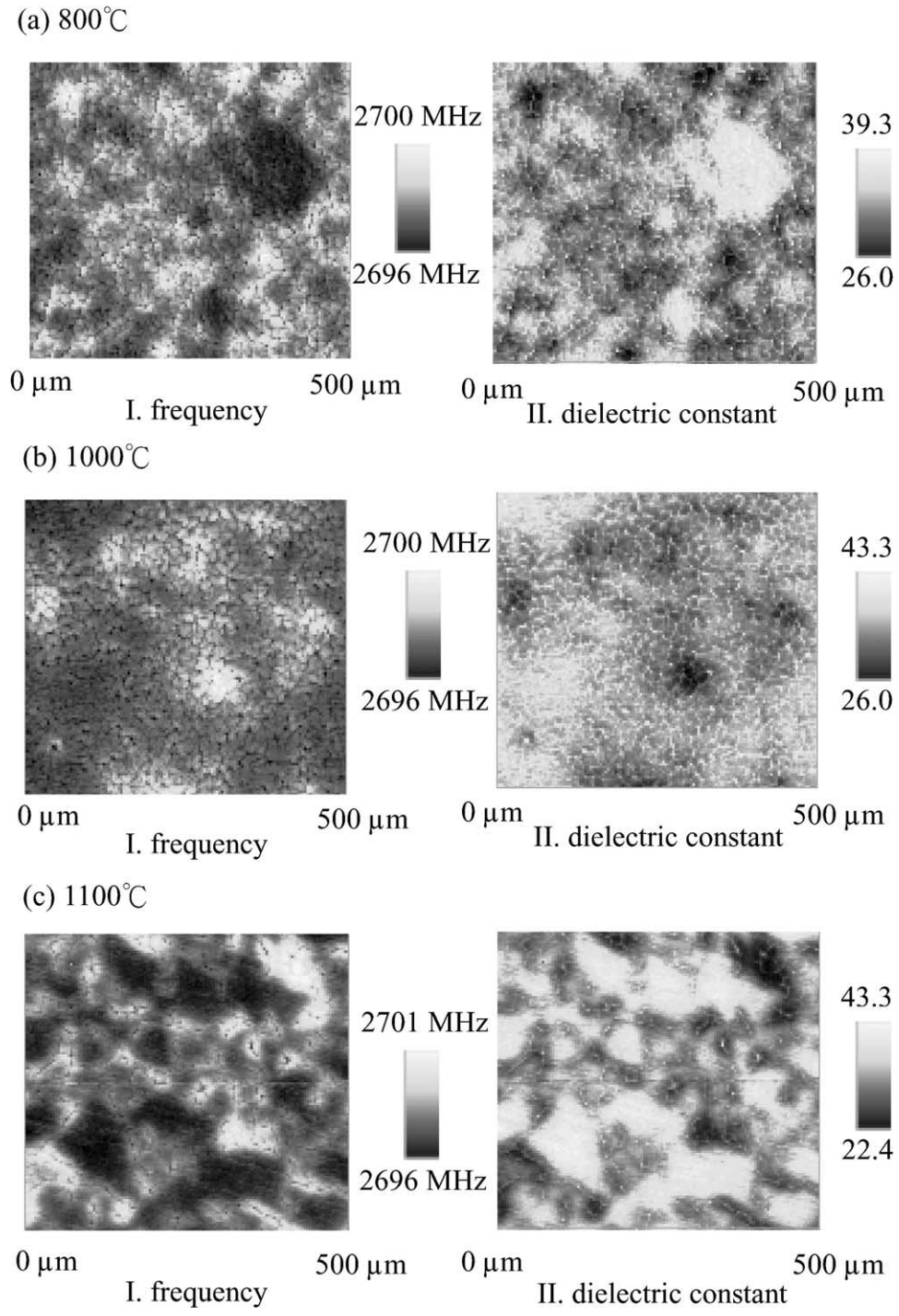

Fig. 3. Frequency images (I) and dielectric constant images (II) for $Ba_2Ti_9O_{20}$ materials prepared from (a) 800 °C, (b) 1000 °C, (c) 1100 °C calcined powders and sintered at 1300 °C (4 h).

the dielectric constant of the 1000 °C-calcined materials shown in Fig. 3b. Apparently, the fluctuation of dielectric constant for the clusters in 800 °C-derived samples can be attributed to the presence of a large proportion of $BaTi_4O_9$ secondary phase (cf. Fig. 1b).

A similar fluctuation of dielectric constant is also observed for the 1100 °C-derived samples (Fig. 3c). The dielectric clusters are even more clearly separated, inferring that they are of different phases. Regions of extremely low dielectric constant ($\varepsilon_r \cong 22.4$) were observed all over the samples, which is presumably the factor resulting in the markedly lower average dielectric constant for these samples (cf. Fig. 1c).

It should be noted that the surface of the samples was polished to a mirror smooth prior to the EMP measurements. Such surface is featureless in SEM

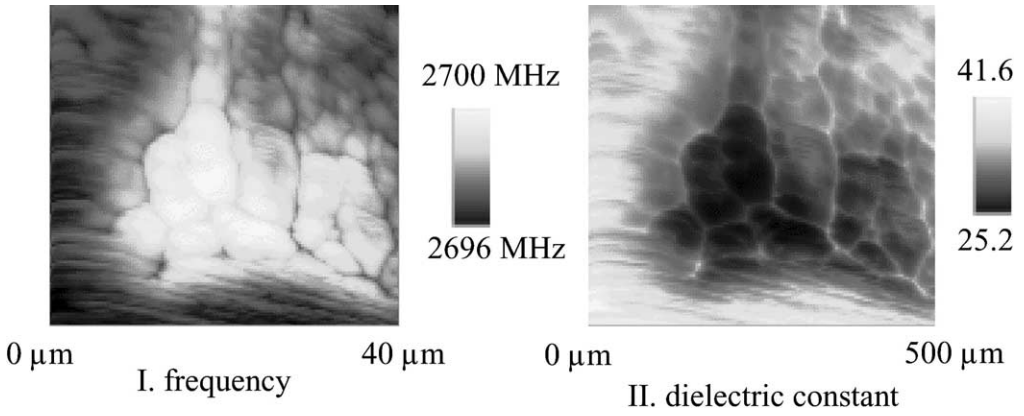

Fig. 4. Frequency images (I) and dielectric constant images (II) for second phase enclosed in Fig. 3c for $Ba_2Ti_9O_{20}$ samples, measured by EMP method.

examinations. SEM images usually were taken after thermal etching and provide the information about the granular structure of the samples. The image derived from the EMP measurements represents the variation of dielectric constant over the samples, which is totally different from the SEM micrographs. To illustrate the special feature of the EMP measurements, the dielectric image of the encircled region (Fig. 3c) was examined using high-resolution modes. In these modes, sharper tips are required, which provide better spatial resolution but lower the accuracy in the dielectric constant values. Fig. 4 shows, again, the frequency image as EMP measured and the dielectric constant image derived from the frequency image, respectively. The low dielectric constant aggregates shown in the center of micrograph, about 25 μm in size, contain several equiaxed clusters about tens of microns, which is at least 10 times larger than the grain size shown in SEM micrographs. Moreover, the high dielectric constant aggregates shown in the left area of the micrograph, also about 25 μm in size, consist of needle-like clusters, about 1 μm in diameter and several tens of microns in length. Most probably the needle-like clusters are $Ba_2Ti_9O_{20}$ grains, whereas the exquiaxed clusters are secondary phases. The nature of these different types of cluster needs further detailed analysis. However, these observations indicate very clearly that the microstructure of the $Ba_2Ti_9O_{20}$ is very complicated and extremely careful processing control is necessary in order to synthesize the materials of good microwave properties.

4. Conclusions

EMP measuring technique has been successfully used to characterize the microwave dielectric properties of $Ba_2Ti_9O_{20}$ ceramics. The average dielectric constants of the images, the macroscopic properties of dielectrics, are in good agreement with results obtained by traditional cavity method. Phase impurity of $Ba_2Ti_9O_{20}$ ceramics can be improved by controlling the calcination conditions. Different phases with different dielectric constants and shapes of grains can be seen directly by EMP. The dielectric images of microstructures are not only consistent with the X-ray diffraction patterns, but also the ε_r values distribute differently between the high Q factor samples and the low Q factor samples.

Acknowledgements

Financial support of National Science Council, R.O.C. through the project NSC 90-2112-M-003-028, NSC-91-2622-E-007-027 and NSC-91-2120-E-003-001 are gratefully acknowledged by the authors.

References

1. Plourde, J. K., Linn, D. F., O'Bryan, H. M. Jr. and Thomson Jr., J., $Ba_2Ti_9O_{20}$ as microwave dielectric resonator. *J. Am. Ceram. Soc.*, 1975, **58**, 418–420.
2. Choy, J. H. and Han, Y. S., Microwave characteristics of BaO–TiO_2 ceramics prepared via a citrate route. *J. Am. Ceram. Soc.*, 1995, **78**, 1169–1172.
3. Lin, W. Y. and Speyer, R. F., Microwave properties of $Ba_2Ti_9O_{20}$ doped with zirconium and tin oxides. *J. Am. Ceram. Soc.*, 1999, **82**, 1207–1211.
4. Wu, J. M. and Wang, H. W., Factors affecting the formation $Ba_2Ti_9O_{20}$. *J. Am. Ceram. Soc.*, 1988, **71**, 869–875.
5. Lahrech, A., Bachelot, R., Gleyzes, P. and Boccara, A. C., Infrared near-field imaging of implanted semiconductors: evidence of a pure dielectric contrast. *Appl. Phys. Lett.*, 1997, **71**, 575–577.
6. Lu, Y., Wei, T., Duewer, F., Lu, Y., Ming, N. B., Schultz, P. G. and Xiang, X. D., High spatial resolution quantitative microwave impedance microscopy by a scanning tip microwave near-field microscope. *Science*, 1997, **276**, 2004–2006.
7. Chen, G., Wei, T., Duewer, F., Lu, Y. and Xiang, X. D., High spatial resolution quantitative microwave impedance microscopy by a scanning tip microwave near-field microscope. *Appl. Phys. Lett.*, 1997, **71**, 1872–1874.
8. Gao, C., Duewer, F. and Xiang, X. D., Quantitative microwave evanescent microscopy. *Appl. Phys. Lett.*, 1999, **75**, 3005–3007.
9. Gao, C. and Xiang, X. D., Quantitative microwave near-field microscopy of dielectric properties. *Review of Scientific Instruments*, 1998, **69**, 3846–3851.